Hindawi
Geofluids
Volume 2021, Article ID 5588248, 11 pages
https://doi.org/10.1155/2021/5588248

Research Article

An Experimental Study on the Particle Size and Shape Distribution of Coal Drill Cuttings by Dynamic Image Analysis

Zhigang Zhang,[1,2] Xiangyun Lan,[1,2] Guangcai Wen,[1,2] Qingming Long,[1,2] and Xuelin Yang[3]

[1]*State Key Laboratory of Gas Disaster Monitoring and Emergency Technology, No. 55, Shangqiao No. 3 Village, Shapingba District, Chongqing, China*
[2]*China Coal Technology Engineering Group Chongqing Research Institute, No. 55, Shangqiao No. 3 Village, Shapingba District, Chongqing, China*
[3]*State Key Laboratory of Coal Mine Disaster Dynamics and Control, College of Resources and Environmental Science, Chongqing University, Chongqing 400044, China*

Correspondence should be addressed to Xiangyun Lan; lanxiangyun@cqccteg.com and Xuelin Yang; yxledu@126.com

Received 3 March 2021; Revised 14 May 2021; Accepted 4 August 2021; Published 21 August 2021

Academic Editor: Jian-Chun Xu

Particle size and shape distribution can be measured in great detail by dynamic image analysis (DIA). The narrow dispersion of repeated experiment results indicates that the particle size distribution can be obtained with high reliability. Particle size distribution can be better fitted to Rosin-Rammler equation than Gaudin-Schuhmann distribution and the lognormal distribution. The spread parameter (m) and the location parameters (d_0) of the Rosin-Rammler equation can be calculated precisely. We analyzed the similarities and differences between the different particle shape distributions. The distributions of form factor and circularity are right-skewed distributions, while the distributions of ellipse ratio, irregularity, and aspect ratio obey a normal distribution. By studying the relation between particle size and shape, we find a linear relationship between the ellipse ratio and the Legendre ellipse diameter on the logarithmic scale.

1. Introduction

Particle size is an important physicochemical parameter of coal. The accurate measurement of particle size distribution (PSD) of coal samples is significant to both scientific research and engineering, such as coal combustion [1–5], coal chemical industry [6–9], adsorption and desorption [10–12], and coal and gas outburst [13, 14]. There are more than one hundred methods and instruments to measure particle size distribution, including sieving, settling velocity measurements, laser diffraction (LD), photon correlation spectroscopy, sound spectrum method, dynamic light scattering method, scanning electron microscope, and X-ray diffraction [15–20]. Of these methods, sieving and LD particle analyzers are widely used for measuring general coal particles (>10 μm) because of their high accuracy, simple operation, fast speed, and high repeatability.

In sieving and LD methods, the shape of particles is usually ignored, and only the single diameter (sieving diameter or sphere diameter) can be obtained. However, for nonspherical particles, a single parameter cannot be used to describe their particle size accurately. Dynamic image analysis (DIA) is a particle size measurement that has been developed rapidly in recent years. Particle size and shape parameters can be obtained precisely and meticulously by analyzing the photos of sample particles by DIA [21–24], which provides a feasible method for the in-depth study of particle size and shape distribution.

As early as the 1980s, some research teams such as Lulea University in Sweden and the University of Arizona in the USA began to use the method of image analysis to measure particle size [25, 26]. Due to the limitation of photography technology and low computing power at that time, the initial technologies of image analysis were generally inaccurate and

it can just measure a small number of particles. With the development of laser light sources, CCD (charge-coupled device) cameras, computer processors, and other hardware facilities, as well as the increasingly mature of the image processing technology, image analysis has made a great progress in the past decade. Now, the dynamic image analyzer is very advanced, and image analysis method has been applied to international technical standards [27]. And measuring particle size by DIA has been gradually applied to geology [28, 29], pharmacy [30], agriculture science [31], mining science [32], and chemistry [33] disciplines. The dynamic image analyzer in this article can photograph millions of sample particles in a few minutes and calculate particle size and shape parameters in several minutes.

2. Experiment

2.1. Samples and Experimental Scheme. The experimental samples are coal drill cuttings from coal seams in Yunnan Hexing Coal Mine of China. Sieve the original coal drill cuttings to 1~3 mm, and then weigh each coal sample in five different masses (5 g, 10 g, 15 g, 20 g, and 25 g), respectively (Figure 1). Then, the particle size and shape distribution of each sample were measured by a dynamic image analyzer, and each measurement was repeated for 8 times.

Figure 1: Experimental samples (coal particles with the sieving diameter of 1~3 mm).

2.2. PSD Measurement. After the sample preparation, the particle size distribution was measured by the OCCHIO ZEPHYR ESR2 particle size analyzer. The basic principle of dynamic image analysis is to continuously photograph the sample particles in their process of motion. Photos are saved in the computer, and an appointed algorithm is used to calculate the specific diameter of each particle, and finally, we can obtain the particle size and shape distribution of the whole sample (Figure 2). We put the sample into the opening funnel. As the feeding chute vibrates mechanically, sample particles fall down from the chute edge. The falling particles are photographed in real time by a CCD camera with telecentric lens, and the photos of all particles are obtained (Figure 3). According to these photos, the particle size and shape parameters are calculated by a specific algorithm, and then, we get the size and shape distribution of coal sample.

The use of a dynamic image analyzer mainly includes the steps of feeding preparation, SOP (standard operation process) setting, display setting, data analysis, and test report exporting. At first, clean the equipment funnel, feeding chute, and glass plate before the experiment to reduce the influence of residue dust on the measurement results. Then, connect the air bottle, vacuum cleaner, and computer workstation to the dynamic image analyzer. Adjust the outlet pressure of air bottle to 300~400 kPa. Pour the coal sample into the funnel, and then turn on the power, open the software in the workstation computer, and set SOP and display parameters:

(1) SOP settings: the SOP settings usually include vibration amplitude, vibration time, photo pixel, photo number, and FPS. In this experiment, we set SOP as follows: the vibration amplitude at the time of prefeeding is 60% for 8 seconds, and the vibration amplitude at the time of photograph is 50%. The number of photos is 50000, and the upper limit of the number of particles is 1500000; air-jet time is 5 s; image FPS is 25. The resolution is 21.8 μm/pixel; frames per second is 25

(2) Display settings: display setting refers to the display content of experimental results, usually including parameter selection of particle size or shape and interval width of the distribution column graph. Display parameters can be adjusted at any time after experiments. To compare the experimental samples with the traditional particle size distribution model, the particle size parameter selected in this experiment is the equivalent volume distribution of the inner diameter (the biggest circle inscribed into the projection area of the particle) [32]. The shape parameters are form factor, ellipse ratio, etc.

After the measurement, the samples are collected for backup. Then, analyze the photos by the software on the workstation computer. When the projections of two or more particles are crossed, manually filter out the "sticky" particles in the photos to reduce the measurement error. Particles in this situation result in the particle size value calculated larger, so the particles can be quickly identified by sorting them from the largest size to the smallest size. A long period of continuous experiments will bring in many micron-sized powder particles to the test system. Since the sieving diameter of the samples in this experiment is 1~3 mm, a funnel filter is added to the measurement software to directly filter out the particles whose particle size is much smaller than 1 mm.

3. Experiment Results

3.1. Comparison of Coal Particle Size Measurement Results of Different Masses. To research the influence of sample mass on the experiment results, each coal sample was divided into five groups according to the mass of 5 g, 10 g, 15 g, 20 g, and 25 g, and every PSD measurement was repeated for 8 times.

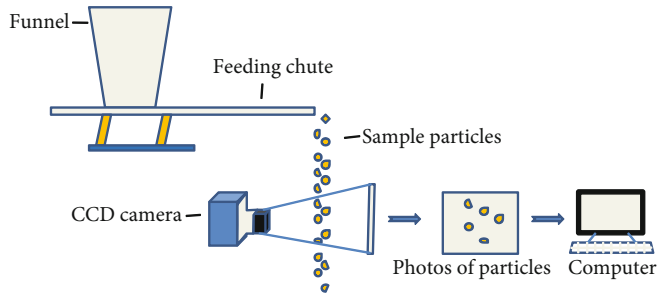

Figure 2: The working principle of dynamic image analyzer.

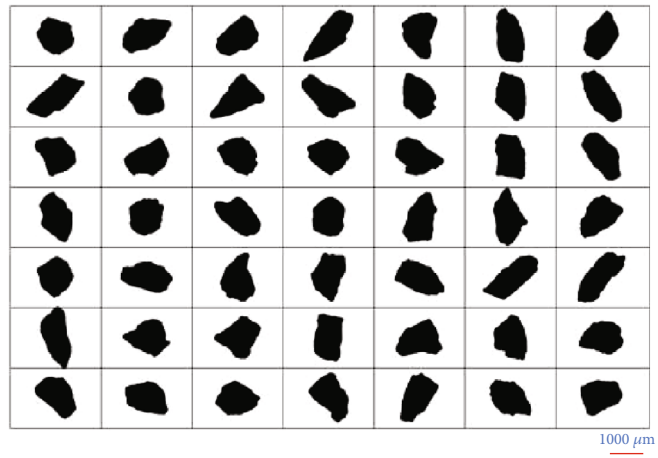

Figure 3: Coal particles photographed by a dynamic image analyzer.

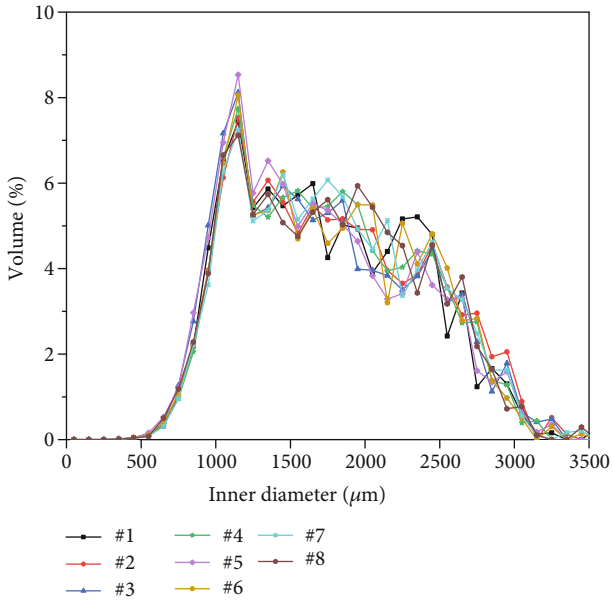

Figure 4: Particle size distribution curve of repeated measurement for 8 times (coal sample mass = 5 g).

Figure 4 shows the particle size distribution curve measured by 8 repeated experiments of coal samples with the mass of 5 g. It can be seen that the distribution trend of the 8 curves is the same.

To analyze the degree of dispersion of the 8 times repeated experiment results, we calculate the statistical parameters (mean value, standard deviation, relative standard deviation, and 95% confidence interval width) of their characteristic parameters of PSD (mean diameter (Mz), median diameter (D50), and sorting coefficient (σ)). Table 1 shows the calculation results of the coal samples with the mass of 5 g. It can be seen that the mean particle size of the repeated experiments is 1832 μm, the standard deviation is 45 μm, and the relative standard deviation is as low as 2%. The half-width of the confidence interval (95% confidence) is as narrow as 38 μm, which means that there is a 95% probability that the truth value of the mean particle size falls within 1831 ± 38 μm.

Similarly, the relative standard deviations of median diameter D50 and the sorting coefficient are also below 5%, and the 95% confidence interval width is also narrow. The small relative standard deviation and narrow 95% confidence interval width mean that even for a small mass of samples (5 g), the particle size distribution measured by the dynamic image analysis method has a high reliability.

Identically, when the masses of coal samples are 10~25 g, the mean value, standard deviation, relative standard deviation, and 95% confidence interval width of the particle size distribution characteristic parameters of 8 times repeated experiments are calculated by the same method (Table 2). It can be seen that as the sample mass changes, the mean particle size of the 8 repeated experiments ranges from 1818 to

Table 1: Statistical parameters (mean, standard deviation, relative standard deviation, and half-width of the 95% confidence interval) of PSD characteristics parameters of 8 times repeated experiments (mass = 5 g).

Measurement number or statistical parameters	Mean diameter (μm)	Median diameter D50 (μm)	Sorting coefficient
1#	1930.09	1905.03	1.60
2#	1820.37	1748.47	1.67
3#	1802.98	1781.41	1.52
4#	1829.04	1746.32	1.69
5#	1829.64	1788.31	1.61
6#	1839.76	1810.73	1.68
7#	1831.06	1748.58	1.68
8#	1770.46	1701.43	1.55
Mean	1831.67	1778.78	1.63
Standard deviation	45.45	60.86	0.07
Relative standard deviation	0.02	0.03	0.04
Half-width of the confidence interval (95% confidence)	38.00	50.88	0.05

Table 2: Statistical parameters of the PSD characteristics of 8 times repeated experiments with different masses (coal sample C1, mass = 5 g~25 g).

Statistical parameters	Sample mass (g)	Mean diameter (μm)	Median diameter D50 (μm)	Sorting coefficient
Mean	5	1831.67	1778.78	1.63
	10	1833.66	1778.66	1.64
	15	1818.41	1749.28	1.67
	20	1822.96	1764.33	1.67
	25	1826.90	1754.92	1.65
Standard deviation	5	45.45	60.86	0.07
	10	42.14	59.41	0.03
	15	41.94	59.40	0.02
	20	41.54	56.30	0.02
	25	40.24	55.03	0.01
Relative standard deviation	5	0.02	0.03	0.04
	10	0.02	0.03	0.02
	15	0.02	0.03	0.01
	20	0.01	0.02	0.01
	25	0.01	0.02	0.01
Half-width of the confidence interval (95% confidence)	5	38.00	50.88	0.05
	10	33.56	52.17	0.02
	15	35.90	59.69	0.02
	20	33.83	54.49	0.02
	25	32.00	54.20	0.01

1834 μm, with a variation range of $(1834 - 1818)/1834 = 0.9\%$. It can be considered that there is little difference of the mean particle size among the different masses. The mean values of the D50 (median diameter) and sorting coefficient of 8 repeated experiments also vary very little with sample mass. As the coal sample mass increases, the relative standard deviation of the repeated experiments of the particle size distribution characteristic parameters decreases slightly. The half-width of the 95% confidence interval is between 32 and 38 um, no more than 1% of the mean value of mean diameter and median diameter D50 (Figure 5). This indicates that the particle size distribution can be precisely measured by the dynamic image analysis method. Even if the mass of the coal sample is small (5 g), the experiment results are credible.

3.2. The PSD Model and Curve Fitting. The mathematical models used to describe the particle size distribution of broken coal samples commonly include the Gaudin-Schuhmann distribution, the Rosin-Rammler distribution,

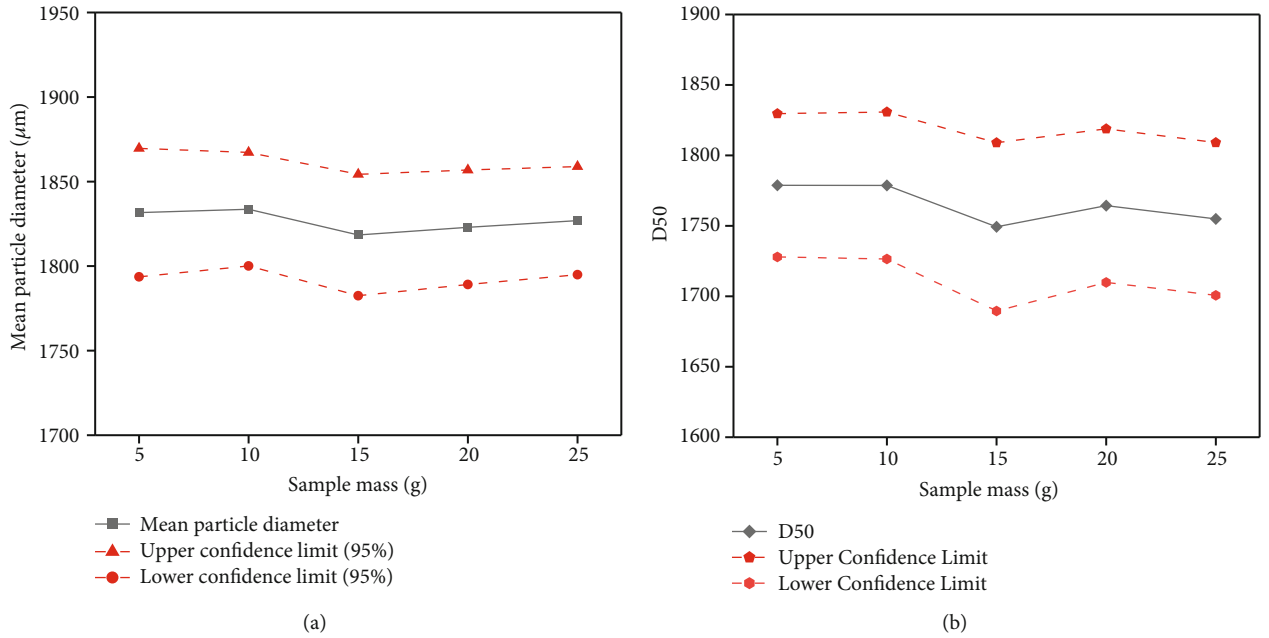

Figure 5: The relationship between the 95% confidence interval width and the sample mass (mean diameter (a) and the median diameter D50 (b); the distance between the upper and lower curves represents the width of the 95% confidence interval).

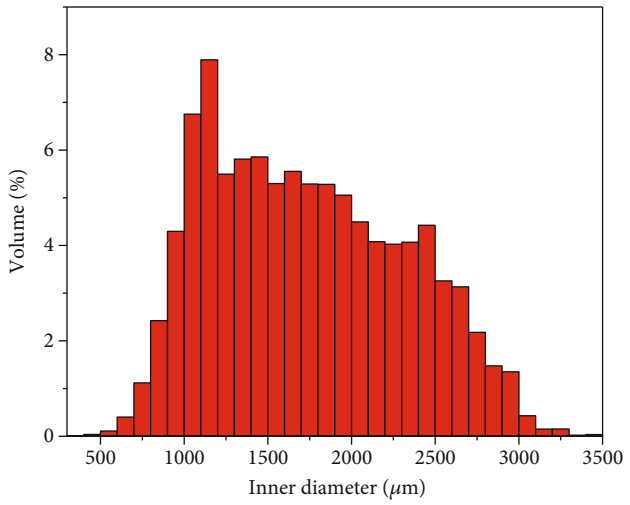

Figure 6: Histogram of coal particle size distribution of the coal sample.

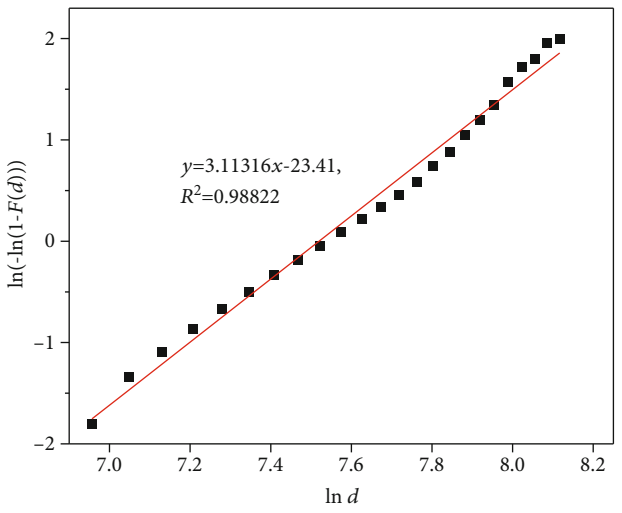

Figure 7: Experimental data and fitting results.

the lognormal distribution, and the fractal particle size distribution [34–36]. The data measured from 8 repeated experiment samples were averaged, and then, we get the particle size distribution histogram of coal samples (Figure 6). It can be seen that the coal sample approximately conforms to the Rosin-Rammler distribution.

The mathematical expression of Rosin-Rammler distribution is [34]

$$F(d) = 100 - 100 \exp\left(-\left(\frac{d}{d_0}\right)^m\right), \quad (1)$$

where $F(d)$ is mass or volume fraction of particles with size smaller than or equal to d (=undersize distribution), assuming constant mass density of all particles (%); d is particle size (μm); d_0 is location parameter of the distribution, with particle size at a volume fraction of 36.8% oversize (μm); and m is the spread parameter of the distribution ($m > 0$).

Take the natural logarithm of equation (1) for two times; we get

$$\ln\{-\ln[1 - F(d)]\} = m \ln d - m \ln d_0. \quad (2)$$

It can be seen that there is a linear relationship between $\ln\{-\ln(1 - F(d))\}$ and $\ln d$. And the spread parameter m

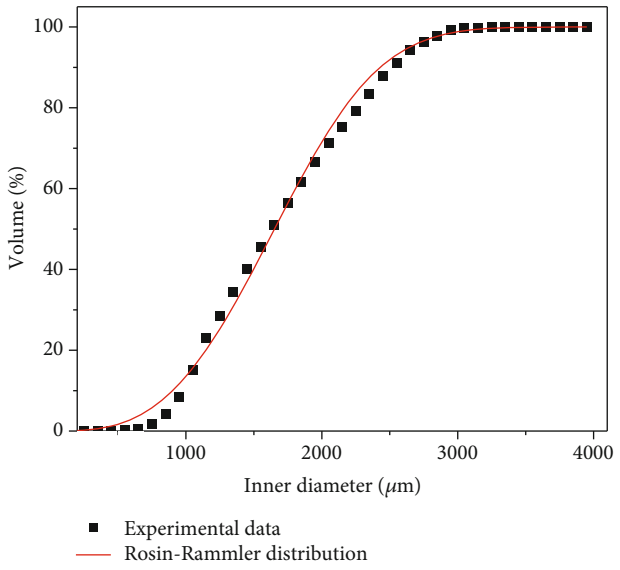

Figure 8: Experimental data and the fitting curve of RR distribution (cumulative distribution).

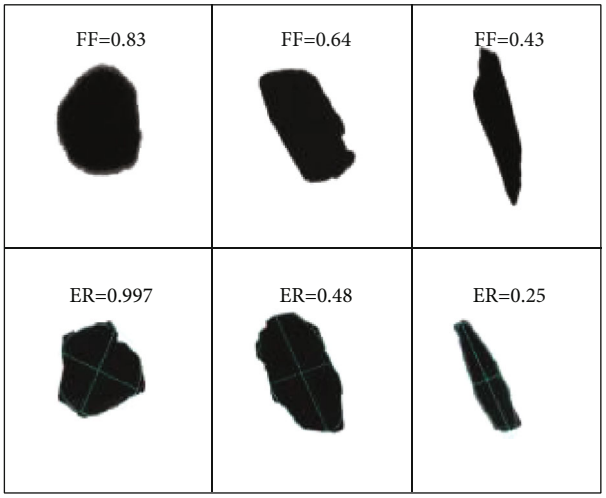

Figure 9: Coal sample particles of different form factors (FF) and ellipse ratio (ER).

and the location parameter d_0 can be obtained according to the slope and intercept of the line. Linear regression was performed on the particle size distribution data obtained from the experiment according to equation (2) (Figure 7). The square of the linear regression correlation coefficient $R^2 = 0.988$, showing a high linear fitting degree. According to the fitting results, the slope of the line (spread parameter m) is 3.11, and the intercept is -23.41. Furthermore, we can calculate the location parameter $d_0 = 1858\,\mu$m.

So far, we obtain the cumulative distribution function of coal particle size of the coal sample:

$$F(d) = 100 - 100 \exp\left(-\left(\frac{d}{1858}\right)^{3.11}\right). \quad (3)$$

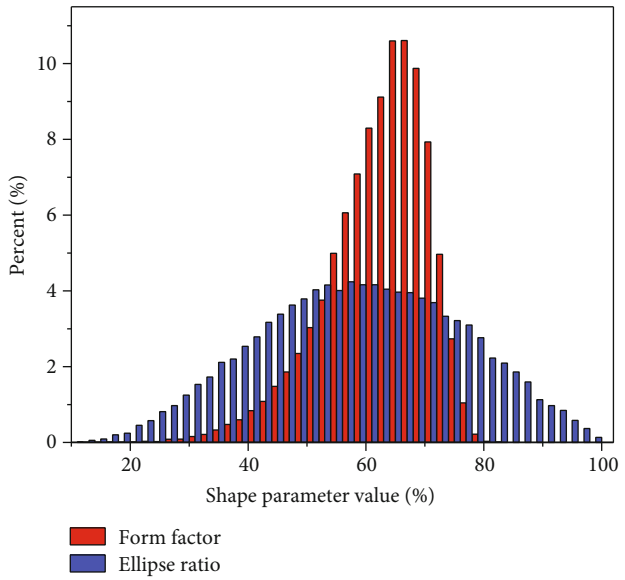

Figure 10: Histogram of particle shape distribution of the form factor and ellipse ratio.

The experimental data and the fitting curve of Rosin-Rammler distribution (equation (3)) are drawn in Figure 8. We can see that the cumulative distribution (also called undersize distribution) of the coal samples measured by the experiment is in good agreement with the Rosin-Rammler distribution.

By differentiating equation (3), the distribution density curve function of the coal sample can be expressed as

$$\begin{aligned} f(d) = F(d)' &= 100 \frac{m}{d_0}\left(\frac{d}{d_0}\right)^{m-1} \exp\left(-\left(\frac{d}{d_0}\right)^{m}\right) \\ &= \left(\frac{d^{2.11}}{1.44 \times 10^{-8}}\right) \exp\left(-\left(\frac{d}{1858}\right)^{3.11}\right). \end{aligned} \quad (4)$$

In dynamic image analysis, the particle size is calculated for each particle. Thus, the particle size distribution is much more detailed and accurate than the sieve method. In theory, the width of the PSD histogram can be as narrow as you want. Therefore, the PSD function can be obtained accurately by fitting the experiment data of DIA.

3.3. Particle Shape Distribution. In the previous calculation related to particle size, we are usually forced to assume that the particle is spherical. The dynamic image method provides an image of each particle, which makes it possible to research the particle shape quantitatively. The application of the particle shape distribution can make some calculations (such as the surface area and the volume of particles) more accurate. There are dozens of parameters to describe the particle shape. In this paper, the form factor (FF) and ellipse ratio (ER) are selected for discussion at first.

The form factor is defined as $FF = 4\pi A/P^2$ (where A is the particle projected area and P is the particle projected perimeter). The definition of form factor includes the projected perimeter of the particle, so it reflects the irregularity of the

Table 3: The definitions of some commonly used particle shape parameters.

Parameter	Definition	Formula
Circularity	The ratio of area-equivalent diameter to the perimeter-equivalent diameter	$\frac{x_A}{x_P}$
Form factor	The ratio of 4π times the projection area to the square of perimeter	$\frac{4\pi A}{P^2}$
Ellipse ratio	The ratio of Legendre ellipse minimum to Legendre ellipse maximum	$\frac{x_{Lmin}}{x_{Lmax}}$
Aspect ratio	The ratio of Feret minimum to Feret maximum	$\frac{x_{Fmin}}{x_{Fmax}}$
Irregularity	The ratio of max-inscribed circle diameter to min-circumscribed circle diameter	$\frac{d_{imax}}{d_{cmin}}$

particle edge and the circular degree of particles in a certain extent. The ellipse ratio is defined as the ratio of Legendre ellipse minimum to Legendre ellipse maximum, which reflects that the particles are rounder or flatter in two dimensions. Figure 9 is a coal particle photo with different form factors or ellipse ratios.

Figure 10 shows the form factor and ellipse ratio distribution histogram of the coal sample. The maximum (minimum) value of the form factor is 0.83 (0.16) and the average value of the form factor is 0.62, indicating that there are no standard spherical particles among the tens of thousands of coal sample particles. The P10 and P90 of the form factor are 0.50 and 0.72 which demonstrates that the form factor of 80% sample particles is between 0.50 and 0.72. The ellipse ratio distribution of the sample is very different from that of the form factor distribution. The ellipse ratio distribution follows a normal distribution with an average value of 0.59 and a variance of 0.029.

Some other commonly used particle shape parameters such as circularity, irregularity, and aspect ratio are shown in Table 3. Figure 11 is the distribution box diagram of those different shape parameters, and each node represents the corresponding particle shape parameter value when the cumulative amount is 10%, 25%, 50%, 75%, and 90%, respectively. The box diagram shows the approximate interval and distribution uniformity of the overall particle shape distribution of the sample. We can see that the circularity distribution is in accord with the form factor distribution, but the value of circularity is bigger (the mean circularity value is 0.79, but the mean form factor is 0.62). The box diagram of circularity is shorter than the form factor, which shows that the circularity distribution is more concentrated than the form factor. The irregularity and aspect ratio distributions are consistent with the ellipse ratio distribution within their respective distribution intervals. They follow a normal distribution, with slightly different mean and variance (the mean/variance of irregularity and aspect ratio are 0.52/0.015 and 0.59/0.022).

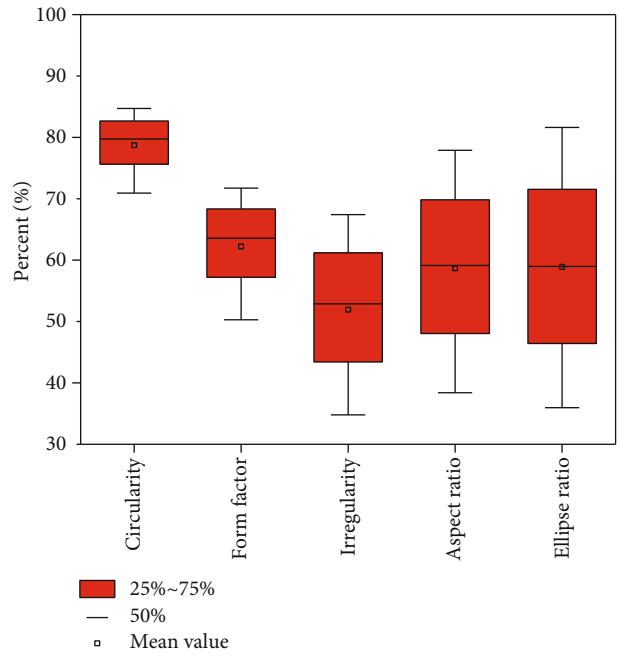

Figure 11: Box diagram of different particle shape distributions (circularity, form factor, irregularity, aspect ratio, and ellipse ratio)

Table 4: Fitted results of different PSD models.

PSD model	Fitted parameters	R^2
Gaudin-Schuhmann	$\alpha = 3.58$, $k = 748$	0.85
The lognormal distribution	$\sigma = 0.45$, $x_a = 1743$	0.90
Rosin-Rammler	$m = 3.11$, $d_0 = 1858$	0.99

4. Discussion

4.1. Comparison of Mathematical Model of Particle Size Distribution. The mathematical models used to describe the particle size distribution of broken coal samples commonly include the Gaudin-Schuhmann distribution, the lognormal distribution, the fractal particle size distribution, and the Rosin-Rammler distribution [34, 37–42].

4.1.1. Gaudin-Schuhmann (GS) Distribution. Assume that the fracture surfaces are completely random by the sight of a straight line starting from a point. The probability of fracture surface numbers within a given distance obeys the Poisson distribution, and then, Gaudin-Schuhmann distribution can be derived as follows [37]:

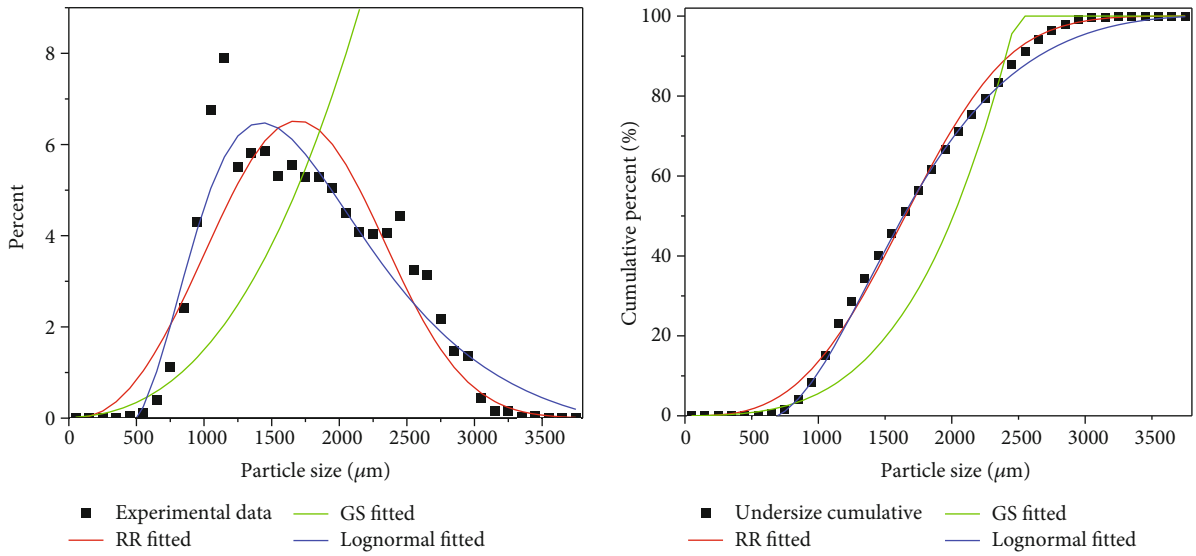

Figure 12: Comparison of different mathematical models of particle size distribution (RR, GS, and lognormal distribution).

$$y = 100\left(\frac{x}{k}\right)^{\alpha}, \tag{5}$$

where y is mass or volume fraction of particles with size smaller than or equal to x (=undersize distribution), assuming constant mass density of all particles (%); x is particle size (μm); k is the distribution characteristic parameter of granularity (μm); and α is the particle size distribution index, dimensionless.

4.1.2. The Lognormal Distribution. Suppose that the breaking probability of any piece in any step is constant when coals are broken and has no concern with the size of the block, the existence of other blocks, or the previous breaking times. And assume that the particle size distribution obtained by simple fragmentation is independent of original size of the block. All fragmentation will be ground into a number normal distribution [38]:

$$\varphi(\ln x) = \frac{1}{\sqrt{2\pi}\sigma}\ \exp\left[-\frac{(\ln x - \ln x_a)}{2\sigma^2}\right], \tag{6}$$

where φ is the distribution probability of granularity in the logarithmic abscissa; x is particle size, (μm); x_a is characteristics of particle size (μm); and σ is a dimensionless distribution characteristic parameter of granularity, dimensionless.

4.1.3. The Fractal Distribution. Fractal distribution can be considered as the result of scale invariance in an abrupt coal broken process of transition from solid state to fragile state. Turcotte [41] used the renormalization group theory and assumed that the breakage probability of each stage was the same to prove that the fractal breakage was generated at similar fracture scales:

$$y = \left(\frac{x}{x_m}\right)^{3-D_t}, \tag{7}$$

where y is mass or volume fraction of particles with size smaller than or equal to x (=undersize distribution); x is particle size (μm); and x_m is characteristics of particle size (μm).

4.1.4. Rosin-Rammler (RR) Distribution. The Rosin-Rammler distribution is an empirical formula to describe the crushing size of coal samples. In 1933, Rosin and Rammler derived a formula to express the particle size distribution of sieved coal dust in Germany [34]. At this time, stimulated by the findings of Rosin and Rammler, Sperling also was working on this subject and derived a similar equation. Next, Bennett examined the correctness of the empirical equation by analyzing many broken coal particles from British mines. The equation of Rosin-Rammler (also called Rosin-Rammler-Sperling-Bennett (RRSB) distribution) is

$$F(d) = 100 - 100\ \exp\left(-\left(\frac{d}{d_0}\right)^m\right), \tag{8}$$

where $F(d)$ is mass or volume fraction of particles with size smaller than or equal to d (=undersize distribution), assuming constant mass density of all particles (%); d is particle size (μm); d_0 is location parameter of the distribution, with particle size at a volume fraction of 36.8% oversize (μm); and m is the spread parameter of the distribution ($m > 0$).

Fitting the experimental data by origin mathematical analysis tools, the particle size distribution of coal samples can be well fitted by RR, GS, and lognormal distribution. The fitted results and correlation coefficients R^2 of different PSD models are shown in Table 4. The fitted curves of the undersize cumulative distribution (or distribution density) are shown in Figure 12. It can be seen that when the particle size distribution is fitted into GS, lognormal, and RR distribution, the correlation coefficients R^2 are 0.85, 0.90, and 0.99, respectively. Therefore, it can be considered that the particle size distribution of broken coal is more consistent with the empirical formula RR distribution.

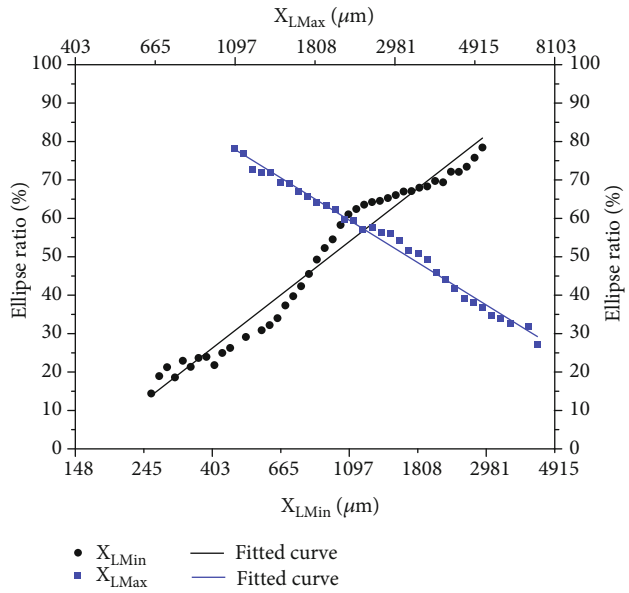

FIGURE 13: Relationship between the Legendre ellipse diameter X_{Lmin} (X_{Lmax}) and ellipse ratio (logarithmic abscissa).

4.2. The Relationship between Particle Size Distribution and Particle Shape Distribution. When analyzing the particle shape of the sample, the authors found that there is a linear relationship between the ellipse ratio and the logarithm of the Legendre ellipse diameter (X_{L}). The experimental data of the Legendre ellipse minimum (maximum) diameter $X_{\mathrm{Lmin}}/(X_{\mathrm{Lmax}})$ and ellipse ratio can be fitted with straight lines on the logarithmic scale (Figure 13), and the correlation coefficient squares R^2 are 0.97 and 0.99.

$$\begin{cases} \mathrm{ER} = 27.7 \ln X_{\mathrm{L\ min}} - 140.1, \\ \mathrm{ER} = -25.7 \ln X_{\mathrm{L\ max}} + 258.0. \end{cases} \quad (9)$$

The ellipse ratio is defined as the ratio of Legendre ellipse minimum diameter to Legendre ellipse maximum diameter ($\mathrm{ER} = X_{\mathrm{Lmin}}/X_{\mathrm{Lmax}}$), which reflects that the particles are rounder or flatter in two dimensions. As the Legendre ellipse minimum diameter increases, the ellipse ratio increases (the molecule increases in the formula), and the projection of the particle on the two-dimensional plane is more similar to a circle. As the Legendre ellipse maximum diameter increases, the ellipse ratio decreases (the denominator increases in the formula), and the projection of the particle on a two-dimensional surface is closer to an ellipse. The theoretical mechanism of this rule is not clear at present, but we can use this linear rule to calculate the surface area and volume of nonspherical particles, which can make the calculation results more accurate.

5. Conclusion

Comparing with different particle size measurement methods, the dynamic image method has the advantages of wide measurement range and good repeatability of measurement results. What is more, the distribution of particle shape distribution can be also obtained during one experiment by DIA. The particle size distribution of the coal sample measured by the dynamic image method is very detailed, and the measured results can be well fitted to the mathematical distribution model. In this paper, the authors use the dynamic image analyzer to measure the particle size and shape distribution of coal drill cuttings and obtain the following conclusions:

(1) The relative standard deviation and 95% confidence interval of PSD characteristic parameters (mean diameter, median diameter, and sorting coefficient) of 8 times repeated experiment results are small and narrow in all different sample mass conditions, which indicates that it is credible for the experimental results measured by dynamic image analysis even though the mass of the experimental sample is small (5 g)

(2) The particle size distribution of coal drill cuttings from coal seams follows the Rosin-Rammler distribution. Taking double logarithms of the cumulative distribution function of the particle size distribution of the coal samples, a straight line can be obtained in the log-abscissa condition of diameter. The square of linear regression correlation coefficient R^2 is 0.988. The spread parameter $m = 3.11$ and the location parameter $d_0 = 1858\,\mu$m can be calculated by the slope and intercept of the line

(3) There are no standard spherical particles among the tens of thousands of coal samples by observing the photos of coal sample particles. The particle shape distribution varies with different shape parameters. The circularity and form factor distribution is a right-skewed distribution. However, the irregularity, aspect ratio, and ellipse ratio distribution obey a normal distribution. There is a linear relationship between the ellipse ratio and the Legendre ellipse diameter (X_{L}) on the logarithmic scale

Data Availability

Experimental data can be obtained by email from the corresponding author.

Disclosure

I would like to declare on behalf of my coauthors that the work described was original research that has not been published previously and not under consideration for publication elsewhere, in whole or in part. Meanwhile, the founding sponsors had no role in the design of the study; in the collection, analyses, or interpretation of the data; in the writing of the manuscript; and in the decision to publish the results.

Conflicts of Interest

The authors declare no conflict of interest.

Authors' Contributions

Zhigang Zhang and Xiangyun Lan analyzed the data and wrote the paper; Guangcai Wen, Xuelin Yang, and Qingming Long did the experiment. The manuscript is approved by all authors for publication. The authors listed have approved the manuscript that is enclosed

Acknowledgments

This study was financially supported by the National Natural Science Foundation of China (51874348, 51574280); Science and Technology Innovation and Entrepreneurship Fund of China Coal Technology Engineering Group (2020-TD-QN014); General Projects of Chongqing Research Institute of China Coal Technology Engineering Group Corporation (2019YBXM28); Chongqing Science Fund for Distinguished Young Scholars (cstc2019jcyjjqX0019); and Chongqing Talent Plan (CQYC201903249).

References

[1] M. W. Mcelroy, R. C. Carr, D. S. Ensor, and G. R. Markowski, "Size distribution of fine particles from coal combustion," *Science*, vol. 215, no. 4528, pp. 13–19, 1982.

[2] X. M. Jiang, H. P. Yang, H. Liu, and C. G. Zheng, "Analysis of the effect of coal powder granularity on combustion characteristics by thermogravimetry," *Proceedings of the CSEE*, vol. 22, no. 12, pp. 142–145, 2002.

[3] Y. Ninomiya, L. Zhang, A. Sato, and Z. Dong, "Influence of coal particle size on particulate matter emission and its chemical species produced during coal combustion," *Fuel Processing Technology*, vol. 85, no. 8-10, pp. 1065–1088, 2004.

[4] Y. Xue, W. Lai, and Z. Wang, "Theoretic analysis of effects of particles sizes on combustion and pyrolysis of coal," *Coal Conversion*, vol. 28, no. 3, pp. 19–21, 2005.

[5] K. Cong, Y. Zhang, F. Han, and Q. Li, "Influence of particle sizes on combustion characteristics of coal particles in oxygen-deficient atmosphere," *Energy*, vol. 170, pp. 840–848, 2019.

[6] M. C. Roco and C. A. Shook, "Modeling of slurry flow: the effect of particle size," *The Canadian Journal of Chemical Engineering*, vol. 61, no. 4, pp. 494–503, 1983.

[7] D. R. Kaushal, K. Sato, T. Toyota, K. Funatsu, and Y. Tomita, "Effect of particle size distribution on pressure drop and concentration profile in pipeline flow of highly concentrated slurry," *International Journal of Multiphase Flow*, vol. 31, no. 7, pp. 809–823, 2005.

[8] Z. Gao, S. Zhu, B. Huang, N. Wang, and C. Guan, "Research on effect of particle size distribution of modified lignite-water slurry," *Coal Preparation Technology*, vol. 1, pp. 1–6, 2009.

[9] R. Xiang, G. Xue, X. Zhang, and P. Chen, "Comparing on the different size of gas coal and lean coal used into coking-blending," *Coal Conversion*, vol. 33, no. 3, pp. 59–62, 2010.

[10] S. Yean, L. Cong, C. T. Yavuz et al., "Effect of magnetite particle size on adsorption and desorption of arsenite and arsenate," *Journal of Materials Research*, vol. 20, no. 12, pp. 3255–3264, 2005.

[11] X. S. Zhang, G. C. Wen, Q. M. Long, and H. Lei, "Experiment study on particle distribution law of seam drilling cuttings," *Coal Science and Technology*, vol. 41, no. 2, pp. 60–63, 2013.

[12] D. Zhao, C. Zhang, H. Chen, and Z. Feng, "Experimental study on gas desorption characteristics for different coal particle sizes and adsorption pressures under the action of pressured water and superheated steam," *Journal of Petroleum Science and Engineering*, vol. 179, pp. 948–957, 2019.

[13] J. Xu, D. Liu, S. Peng, X. Wu, and Q. Liu, "Experimental research on influence of particle diameter on coal and gas outburst," *Chinese Journal of Rock Mechanics and Engineering*, vol. 29, no. 6, pp. 1231–1237, 2010.

[14] K. Wang, L. Wang, F. Du et al., "Influence of coal powder particle sizes on dynamic characteristics of coal and gas outburst," *Journal of China Coal Society*, vol. 44, no. 5, pp. 1369–1377, 2019.

[15] S. Hanson, J. W. Patrick, and A. Walker, "The effect of coal particle size on pyrolysis and steam gasification," *Fuel*, vol. 81, no. 5, pp. 531–537, 2002.

[16] X. L. Yang, G. C. Wen, L. C. Dai, H. T. Sun, and X. Li, "Ground subsidence and surface cracks evolution from shallow-buried close-distance multi-seam mining: a case study in Bulianta Coal Mine," *Rock Mechanics and Rock Engineering*, vol. 52, no. 8, pp. 2835–2852, 2019.

[17] K. Zhang, B. Zhang, J. Liu, D. Ma, and H. Bai, "Experiment on seepage property and sand inrush criterion for granular rock mass," *Geofluids*, vol. 2017, Article ID 9352618, 10 pages, 2017.

[18] F. M. Etzler and M. S. Sanderson, "Particle size analysis: a comparative study of various methods," *Particle & Particle Systems Characterization*, vol. 12, no. 5, pp. 217–224, 1995.

[19] Y. Chen, Z. Ma, D. Ma et al., "Characteristics of the coal fines produced from low-rank coal reservoirs and their wettability and settleability in the Binchang area, South Ordos Basin, China," *Geofluids*, vol. 2021, Article ID 5560634, 17 pages, 2021.

[20] Z. Cao, Y. Ren, Q. Wang, B. Yao, and X. Zhang, "Evolution mechanism of water-conducting channel of collapse column in karst mining area of southwest China," *Geofluids*, vol. 2021, Article ID 6630462, 8 pages, 2021.

[21] A. Persson, "Image analysis of shape and size of fine aggregates," *Engineering Geology*, vol. 50, no. 1-2, pp. 177–186, 1998.

[22] A. K. H. Kwan, C. F. Mora, and H. C. Chan, "Particle shape analysis of coarse aggregate using digital image processing," *Cement and Concrete Research*, vol. 29, no. 9, pp. 1403–1410, 1999.

[23] K. Patchigolla and D. Wilkinson, "Crystal shape characterisation of dry samples using microscopic and dynamic image analysis," *Particle and Particle Systems Characterization*, vol. 26, no. 4, pp. 171–178, 2009.

[24] F. Altuhafi, C. O'Sullivan, and I. Cavarretta, "Analysis of an image-based method to quantify the size and shape of sand particles," *Journal of Geotechnical and Geoenvironmental Engineering*, vol. 139, no. 8, pp. 1290–1307, 2013.

[25] J. Kapur, P. K. Sahoo, and A. Wong, "A new method for gray-level picture thresholding using the entropy of the histogram," *Computer Vision Graphic and Image Processing*, vol. 29, no. 3, pp. 273–285, 1985.

[26] H. Sohn, K. Yun, and H. Chang, "Analysis of image fusion methods using IKONOS imagery," *KSCE Journal of Civil Engineering*, vol. 7, no. 5, pp. 577–584, 2003.

[27] ISO 13322-2, *Particle Size Analysis-Image Analysis Methods-Part 2: Dynamic Image Analysis Methods*, 2008.

[28] N. A. Miller and J. J. Henderson, "Quantifying sand particle shape complexity using a dynamic, digital imaging technique," *Agronomy Journal*, vol. 102, no. 5, pp. 1407–1414, 2010.

[29] J. Luo, G. Huang, Y. Xiong, and L. Zhang, "Experimental study on the relationship between the distribution of micro coal particles and the crushing energy," *Jouranl of China Coal Society*, vol. 41, no. 12, pp. 3054–3061, 2016.

[30] B. Su, Y. Kan, J. Xie, J. Hu, and W. Pang, "Relevance of the pharmacokinetic and pharmacodynamic profiles of Puerariae lobatae Radix to aggregation of multi-component molecules in aqueous decoctions," *Molecules*, vol. 21, no. 7, pp. 845–859, 2016.

[31] Y. Zhang, L. Bai, X. Yang et al., "Application of dynamic iamge particle analysis in determination of corn size and grain size distribution," *Feed Research*, vol. 1, pp. 46–51, 2016.

[32] U. Ulusoy and C. Igathinathane, "Particle size distribution modeling of milled coals by dynamic image analysis and mechanical sieving," *Fuel Processing Technology*, vol. 143, pp. 100–109, 2015.

[33] X. Chen, W. Zhou, X. Cai, Y. Huang, and Y. Yuan, "Particle size distribution measurement of large spray by imaging," *CIESC Journal*, vol. 65, no. 2, pp. 480–487, 2014.

[34] M. Alderliesten, "Mean particle diameters. Part VII. The Rosin-Rammler size distribution: physical and mathematical properties and relationships to moment-ratio defined mean particle diameters," *Particle and Particle Systems Characterization*, vol. 30, no. 3, pp. 244–257, 2013.

[35] X. H. Xu and J. Yu, *The Theory of Rock Crushing*, Coal Industry Publishing House, Beijing, 1984.

[36] Z. Luo, C. Bin, and S. Cheng, "Grain size and shape analysis of beach sediment using dynamic image analysis and comparison with sieving method," *Acta Sedimentologica Sinica*, vol. 34, no. 5, pp. 881–890, 2016.

[37] Q. Wang, Y. Jiang, and J. Hu, "Size and fractal distributions of rock fragments," *China Mining Magazine*, vol. 6, pp. 50–55, 1997.

[38] L. Johannes, D. Franklin, and R. H. Epstein, "Analysis of variance of communication latencies in anesthesia: comparing means of multiple log-normal distributions," *Anesthesia & Analgesia*, vol. 113, pp. 888–896, 2011.

[39] Y. Liu, J. Wang, J. Guo, H. Zhu, and J. Zeng, "Numerical modeling of the conductivity of the particle monolayer with reduced size," *Geofluids*, vol. 2018, Article ID 7073091, 10 pages, 2018.

[40] Y. Chen, B. Yu, K. Zhang, M. Zhang, G. Xu, and Z. Chen, "Permeability evolution and particle size distribution of saturated crushed sandstone under compression," *Geofluids*, vol. 2018, Article ID 6043420, 12 pages, 2018.

[41] D. L. Turcotte, "Fractals and fragmentation," *Journal of Geophysical Research: Solid Earth*, vol. 91, pp. 1921–1926, 1926.

[42] A. Billi and F. Storti, "Fractal distribution of particle size in carbonate cataclastic rocks from the core of a regional strike-slip fault zone," *Geofluids*, vol. 384, no. 1-4, 128 pages, 2004.